IOP Publishing Journal of Optics A: Pure and Applied Optics
J. Opt. A: Pure Appl. Opt. **9** (2007) 649–657 doi:10.1088/1464-4258/9/7/015

Looking at coalescing images and poorly resolved caustics

M V Berry

H H Wills Physics Laboratory, Tyndall Avenue, Bristol BS8 1TL, UK

Received 17 April 2007, accepted for publication 17 May 2007
Published 19 June 2007
Online at stacks.iop.org/JOptA/9/649

Abstract
When looking through a lens of finite aperture, pairs of images associated with caustics, and caustics themselves, are blurred geometrically as well as by diffraction. If the lens aperture is modelled by a Gaussian apodization function, the images in the lens focal plane are Husimi functions of the wave in the plane of the lens, which can be evaluated exactly in terms of Airy and Pearcey functions of complex arguments. Diffraction distorts the spectrum of the source being looked at, even if the geometrical optics is achromatic (as in gravitational lensing); the distortion associated with the images seen as a caustic crosses the lens can be described by the wavelength-dependence of the total light collected by the lens.

Keywords: diffraction, focusing, singularities

1. Introduction

To look means to direct one's gaze in a particular direction, with the eye, or the lens of a telescope, in a particular position. Precise specification of direction and position is incompatible with the wave nature of light, so looking is an emergent notion, becoming precise only in the limit of zero wavelength. According to the standard theory of resolving power [1], the balance between the accuracy of position and direction is determined by the aperture of the lens—controlling, for example, the smallest discernible angular separation between distant objects.

Subtleties arise when images of the same point source coalesce as a caustic crosses the observing lens, or when the 'object' being looked at is itself a caustic. Examples are coalescing reflections of the sun seen in wavy water [2–4], and coalescing images of an astronomical distant source gravitationally lensed by intervening matter [5]. In these situations, imprecise resolution arises not only from diffraction but even at the geometrical level. These are the matters I address here.

It turns out that in the simplest generic cases the image intensity can be expressed in terms of standard diffraction catastrophe functions [6, 7], in which the variables are complex rather than real, and depend only on dimensionless combinations of the lens aperture, the wavenumber of the light, direction angles corresponding to positions in the image plane, and lengths associated with the caustic geometry.

Section 2 sets out the basic theory, in which the incompatible direction and position are regarded as constituting a (slightly unconventional) phase space, and the image intensity emerges as a variant of the Husimi function [8]. Section 3 considers a wave-decorated fold caustic arriving at the lens, corresponding to the coalescence and annihilation of a pair of images of a distant source. As explained in section 4, diffraction generates characteristic distortions of the spectrum of the light, modifying the achromatic images of geometrical optics; these distortions could be a way to observe wave effects in gravitational lensing. If the caustic is in the far field, it can be seen directly in the focal plane of the lens, blurred by the finite lens size as described in section 5 for fold caustics and section 6 for cusp caustics. A numerical illustration is given in section 7.

It is not difficult to extend the theory to describe the smooth transition between the two cases—caustic located in the plane of the lens, and caustic at infinity. But the formulae are simpler and more comprehensible in the limiting cases, so the following will be restricted to these.

It is not my intention here to provide realistic modelling, but to illustrate the phenomena in the simplest manner using closed-form expressions. To achieve this, the lens will be modelled by a Gaussian apodization function, rather than a uniformly transmitting disc with a sharp cutoff at the edge.

The work described here can be regarded as a contribution to aberration theory [1], where images associated with caustics, that are intrinsically distorted, are further degraded by the

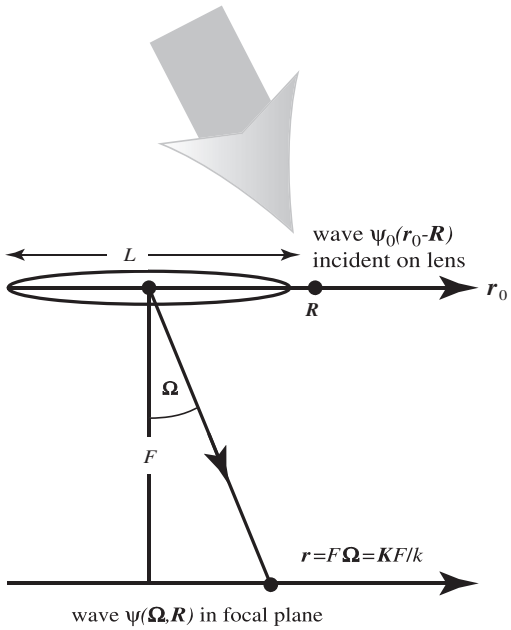

Figure 1. Notation for lens plane, in which the incident wave ψ_0 can be shifted by $\boldsymbol{R}$ relative to the lens of aperture L and focal length F, and the focal plane, where light coming from directions $\boldsymbol{\Omega}$ is imaged.

effects of a finite aperture. Connections between caustics and primary aberrations are described in appendix 2 of [6].

2. Phase space wave and ray formulations of looking

Referring to figure 1, we envisage a wave $\psi_0(\boldsymbol{r}_0 - \boldsymbol{R})$ arriving at points $\boldsymbol{r}_0$ in the plane of a lens, with the shift $\boldsymbol{R}$ denoting displacement of the lens relative to the incident light. Points $\boldsymbol{r}$ in the focal plane correspond to light from direction $\boldsymbol{\Omega}$ or transverse wavevector $\boldsymbol{K}$, where, for wavenumber k and lens focal length F,

$$\frac{\boldsymbol{r}}{F} = \boldsymbol{\Omega} = \frac{\boldsymbol{K}}{k}. \tag{1}$$

The lens has aperture L, and its amplitude transmission function, assumed Gaussian as already stated, is

$$\exp\left\{-\frac{\boldsymbol{r}_0^2}{2L^2}\right\}. \tag{2}$$

For present purposes, paraxial diffraction theory [9, 10] is adequate, and gives the wave arriving in the focal plane in direction $\boldsymbol{\Omega}$ when the lens is displaced by $\boldsymbol{R}$, relative to the incident light, as

$$\begin{aligned}\psi(\boldsymbol{\Omega}, \boldsymbol{R}) &= \frac{k}{2\pi \mathrm{i} F}\int\int \mathrm{d}\boldsymbol{r}_0 \psi_0(\boldsymbol{r}_0 - \boldsymbol{R}) \\ &\quad\times \exp\left\{\mathrm{i}k\frac{(F\boldsymbol{\Omega} - \boldsymbol{r}_0)^2}{2F}\right\}\exp\left\{-\mathrm{i}k\frac{\boldsymbol{r}_0^2}{2F}\right\}\exp\left\{-\frac{\boldsymbol{r}_0^2}{2L^2}\right\} \\ &= \frac{k}{2\pi \mathrm{i} F}\exp\left\{\frac{1}{2}\mathrm{i}kF\Omega^2\right\}\int\int \mathrm{d}\boldsymbol{r}_0 \psi_0(\boldsymbol{r}_0 - \boldsymbol{R}) \\ &\quad\times \exp\{-\mathrm{i}k\boldsymbol{\Omega}\cdot\boldsymbol{r}_0\}\exp\left\{-\frac{\boldsymbol{r}_0^2}{2L^2}\right\}.\end{aligned} \tag{3}$$

Elementary manipulations give the light intensity in the 'phase space' $\boldsymbol{K}, \boldsymbol{R}$ as

$$\begin{aligned}I(\boldsymbol{K}, \boldsymbol{R}) &\equiv \left|\psi\left(\frac{\boldsymbol{K}}{k}, \boldsymbol{R}\right)\right|^2 = \left(\frac{kL}{F}\right)^2 \int\int \mathrm{d}\boldsymbol{r}_0 \int\int \mathrm{d}\boldsymbol{q}_0 \\ &\quad\times W_0(\boldsymbol{r}_0, \boldsymbol{q}_0)\exp\left\{-\frac{(\boldsymbol{r}_0 + \boldsymbol{R})^2}{L^2} - (\boldsymbol{q}_0 - \boldsymbol{K})^2 L^2\right\},\end{aligned} \tag{4}$$

where W_0 is the Wigner function [8] of the incident light, defined by

$$\begin{aligned}W_0(\boldsymbol{r}_0, \boldsymbol{q}_0) &= \frac{1}{(2\pi)^2}\int\int \mathrm{d}\boldsymbol{\xi}\,\psi_0^*\left(\boldsymbol{r}_0 + \frac{1}{2}\boldsymbol{\xi}\right)\psi_0\left(\boldsymbol{r}_0 - \frac{1}{2}\boldsymbol{\xi}\right) \\ &\quad\times \exp\{\mathrm{i}\boldsymbol{q}_0\cdot\boldsymbol{\xi}\}.\end{aligned} \tag{5}$$

For calculations of Wigner functions corresponding to diffraction decorating canonical caustics, and unexpected integral relations involving their projections, giving the associated wave intensity (without the aperture effect considered here) see [11].

Two obvious limiting cases can easily be derived. As $L \to \infty$, corresponding to an unobstructed lens, the exponential involving $\boldsymbol{q}_0$ in (4) becomes a delta-function, and I is the square of the Fourier transform of ψ_0, evaluated at $\boldsymbol{K}$. As $L \to 0$, corresponding to a 'lens' of infinitesimal aperture ('Gaussian pinhole camera'), the exponential involving $\boldsymbol{r}_0$ in (4) becomes a delta-function, and the focal plane is illuminated by a broad Gaussian, with width $1/(kL)$ and intensity $|\psi_0(-\boldsymbol{R})|^2$.

According to (4) and (5), the lens acts to produce an image by Gaussian smoothing of the incident Wigner function, with the difference that the variables $\boldsymbol{R}$ and $\boldsymbol{K}$ refer to different planes, so (4) involves $+\boldsymbol{R}$ rather than $-\boldsymbol{R}$. Therefore the image intensity is the Husimi function [8] of the incident light, with variables $-\boldsymbol{R}$, $\boldsymbol{K}$. Although in what follows all of the incident waves ψ_0 will represent coherent light, the result (4) also applies to incoherent light. (For a different optical application of the Husimi function, see [12].)

In the geometrical-optics limit $k \to \infty$, the Wigner function can be replaced by the geometrical ray density in the phase space $\boldsymbol{r}_0$, $\boldsymbol{\Omega}_0$:

$$W_0(\boldsymbol{r}_0, k\boldsymbol{\Omega}_0) \to \frac{1}{k^2} W_{0\mathrm{geom}}(\boldsymbol{r}_0, \boldsymbol{\Omega}_0). \tag{6}$$

For coherent light, $W_{0\mathrm{geom}}$ is a delta-function selecting the ray(s) incident on the lens in the direction $\boldsymbol{\Omega}_0$ at the position $\boldsymbol{r}_0$. In (4), the exponent involving $\boldsymbol{q}_0$ is large (as in the large-L limit mentioned above), and the corresponding exponential acts like a delta-function, so $\boldsymbol{q}_0$ can be replaced by $\boldsymbol{K}$, leading to the simple expression

$$\begin{aligned}I_{\mathrm{geom}}(\boldsymbol{\Omega}, \boldsymbol{R}) &= \frac{1}{F^2}\int\int \mathrm{d}\boldsymbol{r}_0 W_{0\mathrm{geom}}(\boldsymbol{r}_0, \boldsymbol{\Omega}) \\ &\quad\times \exp\left\{-\frac{(\boldsymbol{r}_0 + \boldsymbol{R})^2}{L^2}\right\}.\end{aligned} \tag{7}$$

For one-dimensional incident light, in which ψ_0 depends on a single coordinate, for example $x - X$, the above formulae can be simplified by writing all integrals as single rather than double, and replacing all prefactors by their square roots.

We note also that the results (3)–(5) also give the wave produced in the far field when a Gaussian beam illuminates an object with complex transmission amplitude $\psi_0(\boldsymbol{r}_0 - \boldsymbol{R})$. Canonical caustics seen through an aperture with a sharp edge

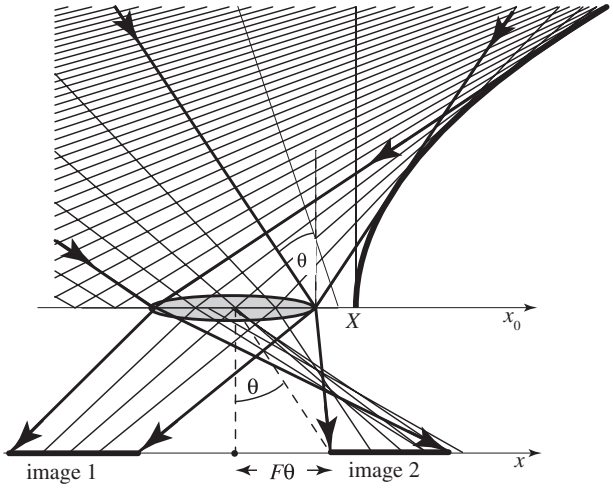

Figure 2. Formation of two images by rays focused onto a caustic curve. Each image is spread as illustrated in figure 3, and the rays shown in bold are those encountering the edges of the lens.

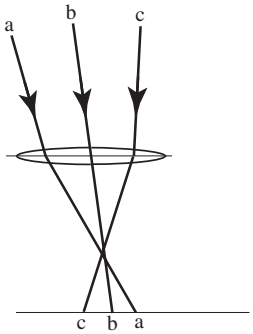

Figure 3. Geometrical spread of each image from rays arriving in different directions across the lens.

(rather than an apodized aperture as here) were explored by Nye [13–15], who described in detail the transitions from diffraction catastrophes to the Airy rings as L decreases from large to small values. In some respects, the work reported here is complementary to his.

3. Two coalescing images as caustic crosses lens

Consider a caustic intersecting the lens plane perpendicularly at $x_0 = X$, as illustrated in figure 2 (generalization to non-perpendicular intersection is easy but adds inessential complication). Points $x_0 < X$ in the lens plane are reached by two rays, while no rays reach points $x_0 > X$. Each of the two rays reaching x_0 contributes to a different member of the pair of images in the focal plane. The rays forming image 1 have touched a real caustic, while those forming image 2 are associated with a virtual caustic. Since the direction of each ray varies across the lens, the images are broadened as indicated in figure 3; this geometrical broadening is greater for larger L. The rays satisfy

$$x_0 - X + A\theta_0^2 = 0, \tag{8}$$

and it follows from elementary geometry that A is half the radius of curvature of the caustic in the lens plane.

The incident wave decorating the fold caustic of figure 2 can be written in terms of the Airy function, as

$$\psi_0(x_0 - X) = (kA)^{1/6}\mathrm{Ai}\left(\frac{k^{2/3}}{A^{1/3}}(x_0 - X)\right). \tag{9}$$

Here $X = 0$ corresponds to the caustic intersecting the centre of the lens, and the powers of k are chosen in accordance with the diffraction catastrophe exponents [6, 16], to make ψ_0 of order unity in the geometrical regime $x_0 \ll X$ of two interfering rays, and to make the fringe width near the caustics scale as $k^{-2/3}$. Thus the image wave is given by the integral (cf equation (3))

$$\begin{aligned}\psi(\theta, X) = {} & \sqrt{\frac{k}{2\pi \mathrm{i}F}}(kA)^{1/6}\exp\left\{\frac{1}{2}\mathrm{i}kF\theta^2\right\} \\ & \times \int_{-\infty}^{\infty}\mathrm{d}x_0\mathrm{Ai}\left(\frac{k^{2/3}}{A^{1/3}}(x_0 - X)\right)\exp\{-\mathrm{i}k\theta x_0\} \\ & \times \exp\left\{-\frac{x_0^2}{2L^2}\right\}.\end{aligned} \tag{10}$$

Evaluation is straightforward when the Airy function is written in terms of its integral representation. The result is conveniently expressed in terms of the following dimensionless angle and wavenumber variables, each also involving the lens aperture L:

$$\gamma \equiv \theta\sqrt{\frac{A}{L}}, \qquad \xi \equiv \frac{X}{L}, \qquad \kappa \equiv k\sqrt{\frac{L^3}{A}}, \tag{11}$$

and leads to

$$I(\theta, X) = \frac{A}{2\pi F}J(\gamma, \xi, \kappa), \tag{12}$$

where

$$\begin{aligned}J(\gamma, \xi, \kappa) = {} & 2\pi\kappa^{4/3}\exp\left\{-\kappa^2\left(\gamma^2 + \xi - \tfrac{1}{6}\kappa^2\right)\right\} \\ & \times \left|\mathrm{Ai}\left(\kappa^{2/3}\left(-\xi + \mathrm{i}\kappa\gamma + \tfrac{1}{4}\kappa^2\right)\right)\right|^2.\end{aligned} \tag{13}$$

The corresponding geometrical-optics images can be found either from the asymptotics of the Airy function for large positive argument [17], or from (7), with the classical phase-space density (cf (8))

$$W_{0\mathrm{geom}}(x_0, \theta_0) = \frac{A}{2\pi}\delta(x_0 + A\theta_0^2). \tag{14}$$

Either way leads to

$$J_{\mathrm{geom}}(\gamma, \xi) = \exp\left\{-(\xi - \gamma^2)^2\right\} = \exp\left\{-\frac{(X - A\theta^2)^2}{L^2}\right\}. \tag{15}$$

The broadened geometric images are centred on $\gamma = \pm\sqrt{\xi}$, i.e. $\theta = \pm\sqrt{(X/A)}$, and have widths $\Delta\gamma \sim 1/\sqrt{\xi}$, i.e. $\Delta\theta \sim L/\sqrt{(AX)}$.

Figure 4 shows the images as functions of scaled direction γ and caustic position ξ, for different values of κ, with the pair of broadened images emerging more clearly for increasing ξ as κ increases, i.e. as k or L increase. Figure 5 illustrates the emergence of the geometrical limit in more detail, by concentrating on the images for a particular value of ξ.

In the opposite limit of small $\boldsymbol{\kappa}$ (poorly resolved images), it is clear from figures 4(a) and (b) that the images have merged (rather than emerged) and are replaced by the oscillations of

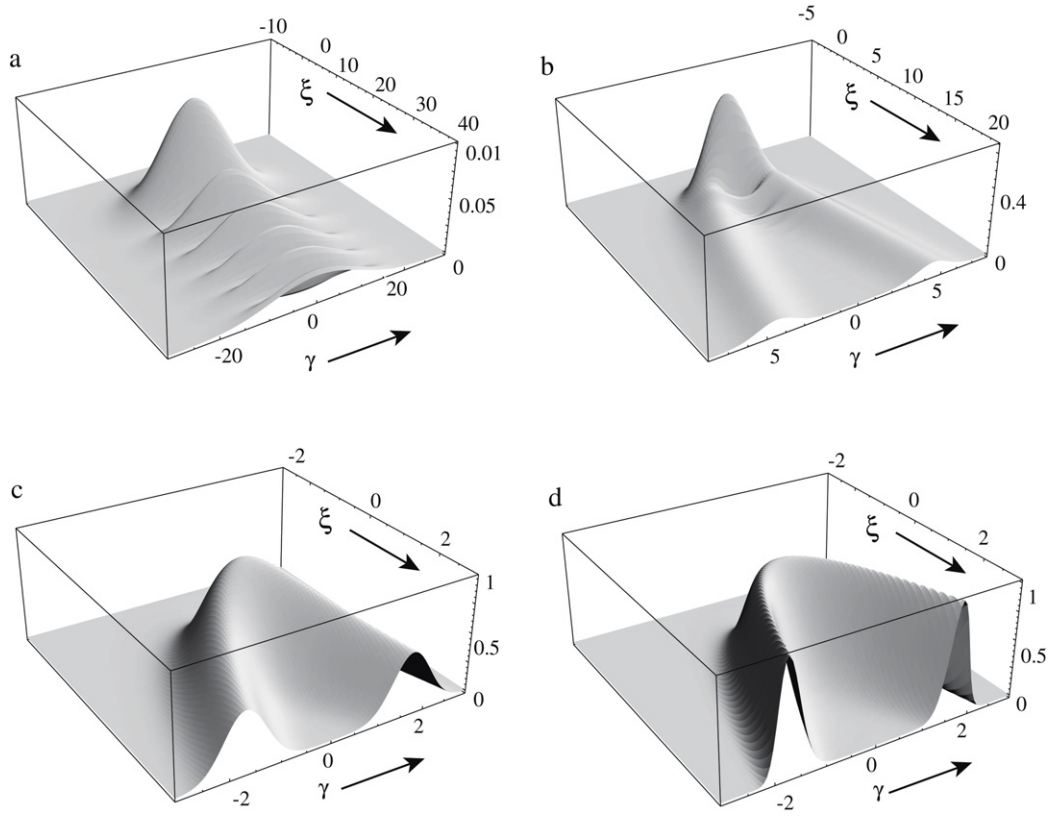

Figure 4. Image intensity $J(\gamma, \xi, \kappa)$ (equation (13)) in direction space γ and caustic position ξ, for (a) $\kappa = 0.1$, (b) $\kappa = 0.7$, (c) $\kappa = 2$, (d) the geometrical-optics intensity $J_{\text{geom}}(\gamma, \xi)$ (equation (15)).

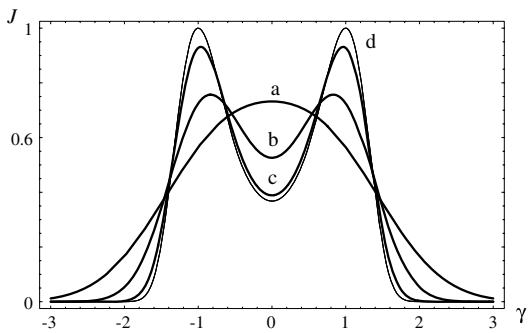

Figure 5. Images $J(\gamma, 1, \kappa)$ as functions of γ, for (a) $\kappa = 1$, (b) $\kappa = 2$, (c) $\kappa = 5$, (d) $J_{\text{geom}}(\gamma, 1)$.

the Airy function for positive ξ, resulting from interference between the two rays. This is an illustration of the complementarity between wave interference and the separation of geometrical images, familiar in quantum mechanics as the uncertainty principle.

The zeros of the Husimi function (13), so important in other contexts [8], are here just the zeros of the Airy function. They are located at $\gamma = 0$, ξ_n; as κ increases, all ξ_n recede towards $+\infty$, into the Gaussian tail of the intensity.

As a numerical example, consider looking at a pair of coalescing images of the sun (regarded as a point) reflected in wavy water with profile $H \sin(2\pi x/\Lambda)$. By expanding about one of the inflection points, it is easy to calculate the curvature of the caustic at height Z (the lens plane, where the eye is situated) and hence the parameter A in (8) and (9): $A = 4\pi^3 H Z^3/\Lambda^3$. Then, for visible light, and eye pupil size $L \approx 2$ mm, water wavelength $\Lambda = 1$ m and wave height $H = 0.1$ m, viewed from $Z = 10$ m, the dimensionless wavenumber (11) is $\kappa \approx 10$, which is comfortably in the geometrical regime; for the smaller wave $\Lambda = 0.1$ m, $H = 0.03$ m, $\kappa \approx 0.3$, which is in the interference regime.

4. Spectral distortion near caustic

Since diffraction is essentially wavelength-dependent, the spectrum of images of a polychromatic source will be distorted as the caustic crosses the lens. This is in addition to any geometrical distortion, ignored here, caused by propagation in a dispersive medium. Since gravitational lensing is geometrically achromatic [5], the diffractive spectral distortion discussed in this section might be a way to detect associated wave effects (see also [18–20]).

A function quantifying spectral distortion, which could be useful even when the separate images cannot be resolved, is the integrated intensity across the image, namely

$$S(\xi, \kappa) \equiv \int_{-\infty}^{\infty} \mathrm{d}\gamma\, J(\gamma, \xi, \kappa)$$
$$= 2\pi\kappa^{1/3} \int_{-\infty}^{\infty} \mathrm{d}u\, \mathrm{Ai}^2\left(\kappa^{2/3}(u - \xi)\right) \exp(-u^2). \qquad (16)$$

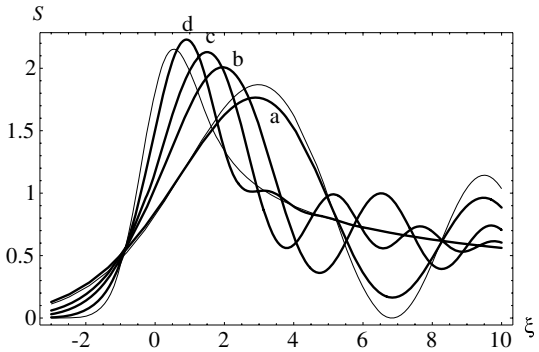

Figure 6. Bold curves: spectral distortion function $S(\xi, \kappa)$ for (a) $\kappa = 0.2$, (b) $\kappa = 0.35$, (c) $\kappa = 0.5$, (d) $\kappa = 1$. The thin curve close to (a) is the small-k approximation (18), and the thin curve close to (d) is the $k \to \infty$ limit $S_{\rm geom}(\xi)$ (equation (17)).

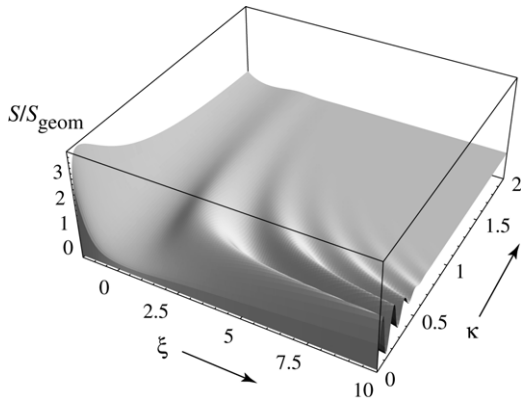

Figure 7. Relative spectral distortion function $S(\xi, \kappa)/S_{\rm geom}(\xi)$.

The geometrical-optics limit is

$$S_{\rm geom}(\xi) \equiv \int_{-\infty}^{\infty} {\rm d}\gamma\, J_{\rm geom}(\gamma, \xi) = \sqrt{\frac{|\xi|}{2}} \exp\left(-\frac{1}{2}\xi^2\right)\left[K_{1/4}\left(\frac{1}{2}\xi^2\right) + \Theta(\xi)\pi\sqrt{2} I_{1/4}\left(\frac{1}{2}\xi^2\right)\right], \tag{17}$$

and the opposite limit is

$$S(\xi, \kappa) \approx 2\pi^{3/2}\kappa^{1/3}{\rm Ai}^2(-\kappa^{2/3}\xi) \qquad (\kappa \ll 1). \tag{18}$$

Figure 6 shows how the integrated intensity changes as the caustic crosses the lens, for different values of κ. Figure 7 shows the relative spectral distortion $S(\xi, \kappa)/S_{\rm geom}(\xi)$. The distortion is much greater for negative ξ, that is on the dark side of the caustic, where the wave is evanescent, so the longer wavelengths penetrate more. Simply stated, images are reddened on the dark sides of caustics. (Rainbows—the most familiar caustics—are reddened on their dark sides too [21], but unless the raindrops are very small this effect is the result of dispersion rather than diffraction.)

5. Poorly resolved far-field fold caustic

Caustics in the far field can be generated by a wave ψ_0, in the lens plane, that corresponds to a pure phase variation, i.e. constant amplitude; the far-field caustics are the images of the contours of zero Gaussian curvature of the phase [22]. An everyday example is virtual caustics seen on rainy nights by people wearing spectacles, when the illumination is that of a distant lamp and the phase variation is produced by irregularly shaped raindrop 'lenses' on the glass lenses [7, 22]. Visibility of these caustics is limited by the finite size of the water-drops or the pupil of the eye (as well as the finite size of the source which we do not consider here). By the duality described in the last paragraph of section 2, similar images (now real rather than virtual) can be produced on a distant screen when a Gaussian laser beam illuminates water-drops on a glass plate, or smoothly undulating bathroom-window glass [6].

For simplicity, we henceforth drop the X dependence, and consider only $X = 0$, that is, caustics centrally situated relative to the lens. The simplest case is a fold caustic in the far field, for which a local model is

$$\psi_0(x_0) = \exp\left\{{\rm i}k\frac{x_0^3}{3A^2}\right\}. \tag{19}$$

The corresponding rays in the lens plane are

$$x_0^2 - A^2\theta_0 = 0, \tag{20}$$

so the length A describes the quadratic spread of ray directions near the point x_0 that generates the caustic. Equation (20) resembles the expression (8) describing a caustic in the lens plane; but the similarity is superficial, because with (20) only one ray direction corresponds to each position, rather than two or zero as with (8).

Convenient dimensionless direction and wavevector variables are (cf (11))

$$\gamma \equiv \frac{A^2}{L^2}\theta, \qquad \kappa \equiv \frac{L^3}{A^2}k. \tag{21}$$

The one-dimensional integral corresponding to (3) is easily evaluated, with the result that the poorly resolved fold intensity is

$$I(\theta) = \frac{A^2}{FL} J(\gamma, \kappa), \tag{22}$$

where

$$J(\gamma, \kappa) = 2\pi\kappa^{1/3}{\rm Ai}^2\left(-\kappa^{2/3}\gamma + \frac{1}{4\kappa^{4/3}}\right)\exp\left\{\frac{1}{6\kappa^2} - \gamma\right\}. \tag{23}$$

In the large L limit, $\gamma \to 0$ and $\kappa \to \infty$, but $\kappa^{2/3}\gamma$ is independent of L, so J is simply the perfectly resolved Airy intensity.

The geometrical limit $\kappa \gg 1$ can be obtained from the asymptotics of the Airy function for large negative argument, followed by an average over the fast interference oscillations. This gives

$$J_{\rm geom}(\gamma) = \frac{\exp(-\gamma)}{\sqrt{\gamma}}\Theta(\gamma) = \frac{L}{A\sqrt{\theta}}\exp\left\{-\frac{A^2}{L^2}\theta\right\}\Theta(\theta), \tag{24}$$

in which Θ denotes the unit step. An alternative derivation is via (7) and the phase-space density (cf (20))

$$W_{0\rm geom}(x_0, \theta_0) = \delta\left(\frac{x_0^2}{A^2} - \theta_0\right). \tag{25}$$

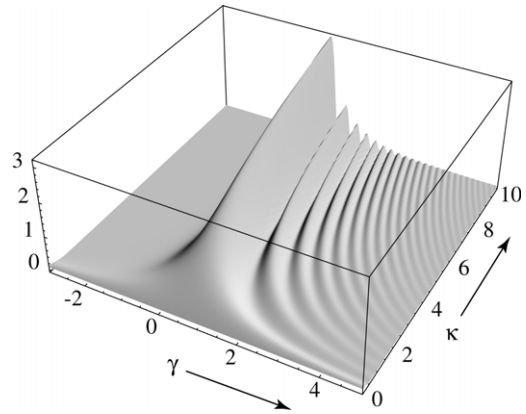

Figure 8. Far-field fold intensity $J(\gamma, \kappa)$.

The small-L limit, obtained from the asymptotics of the Airy function for large positive argument, is

$$J(\gamma,\kappa) \approx \kappa \exp(-\gamma^2\kappa^2) \propto \exp(-L^2k^2\theta^2) \qquad (\kappa \ll 1). \tag{26}$$

Figure 8 shows the intensity as a function of γ and κ, illustrating the transition between the geometrical and small-L limits. As κ decreases, the Airy zeros recede towards positive γ, and are eventually lost in the tail of the Gaussian (26). Figure 9 illustrates the extreme cases. A numerical example will be given in section 7.

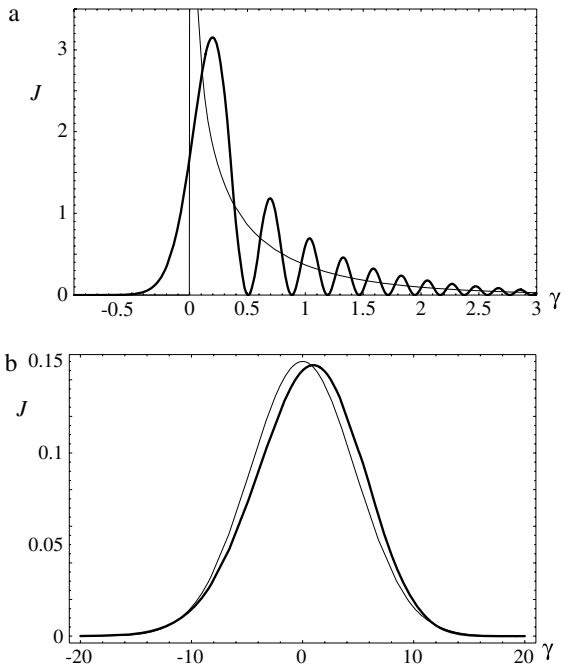

Figure 9. Thick curves: far-field fold intensity $J(\gamma, \kappa)$ for (a) $\kappa = 10$, (b), $\kappa = 0.15$. Thin curves: (a) the $k \to \infty$ limit $J_{\text{geom}}(\gamma)$ (equation (24)), (b) small κ approximation (26). In (a) the geometrical limit emerges only after averaging over the fast interference oscillations.

6. Poorly resolved far-field cusp caustic

The wave

$$\psi_0(\boldsymbol{r}_0) = \exp\left\{ik\left(\frac{x_0^2}{2A} + \frac{x_0y_0^2}{B^2}\right)\right\}, \tag{27}$$

in the lens plane, generates a cusp in the far field. With angles defined by

$$\boldsymbol{\Omega} \equiv \{\theta, \phi\}, \tag{28}$$

the caustic is easily shown to be

$$\theta^3 = \frac{27B^2}{16A^2}\phi^2. \tag{29}$$

The constants A and B are lengths related to the caustic geometry.

Convenient dimensionless parameters are

$$\gamma \equiv \frac{A}{L}\theta, \qquad \delta \equiv \frac{A}{L}\phi, \qquad \sigma \equiv \frac{B}{\sqrt{AL}}, \qquad \kappa \equiv \frac{L^2}{A}k. \tag{30}$$

In terms of these, the cusp is

$$\gamma^3 = \frac{27\sigma^2}{16}\delta^2. \tag{31}$$

Inserting the lens-plane wave (27) into the formulae of section 2 gives, after some algebra, the poorly resolved cusp in terms of the Pearcey function [7, 23, 24], defined by

$$P(u,v) = \int_{-\infty}^{\infty} \mathrm{d}t \exp\left\{\mathrm{i}(t^4 + vt^2)\right\} = \int_0^{\infty\exp(\mathrm{i}\pi/8)} 2\,\mathrm{d}t \cos(ut)\exp\left\{\mathrm{i}(t^4 + vt^2 + ut)\right\}, \tag{32}$$

where the second form is convenient for numerical evaluation because the deformation of the path makes the integrand decay as $\exp(-|t|^4)$.

The Pearcey variables are

$$u = \delta\sigma\sqrt{\kappa}[2(\kappa - \mathrm{i})]^{1/4}, \qquad v = -\gamma\kappa\sqrt{\frac{2}{\kappa - \mathrm{i}}} + \mathrm{i}\frac{\sigma^2}{\kappa}\sqrt{\frac{(\kappa - \mathrm{i})}{2}}, \tag{33}$$

leading to the intensity

$$I(\boldsymbol{\Omega}) = \left(\frac{A}{\pi F}\right)^2 J(\gamma, \delta, \sigma, \kappa), \tag{34}$$

where

$$J(\gamma,\delta,\sigma,\kappa) = \frac{\kappa\sigma^2}{\pi\sqrt{2}(\kappa^2+1)^{1/4}}|P(u,v)|^2 \exp\left\{-\frac{\gamma^2\kappa^2}{\kappa^2+1}\right\}. \tag{35}$$

In the large L limit, $\gamma \to 0$, $\delta \to 0$, $\sigma \to 0$ and $\kappa \to \infty$, but $\kappa^{1/2}\gamma$ and $\kappa^{3/4}\delta\sigma$ are independent of L, so J is simply the perfectly resolved Pearcey intensity.

The Gaussian limit for small L comes from the asymptotic evaluation of P for large v and small u, and is dominated by

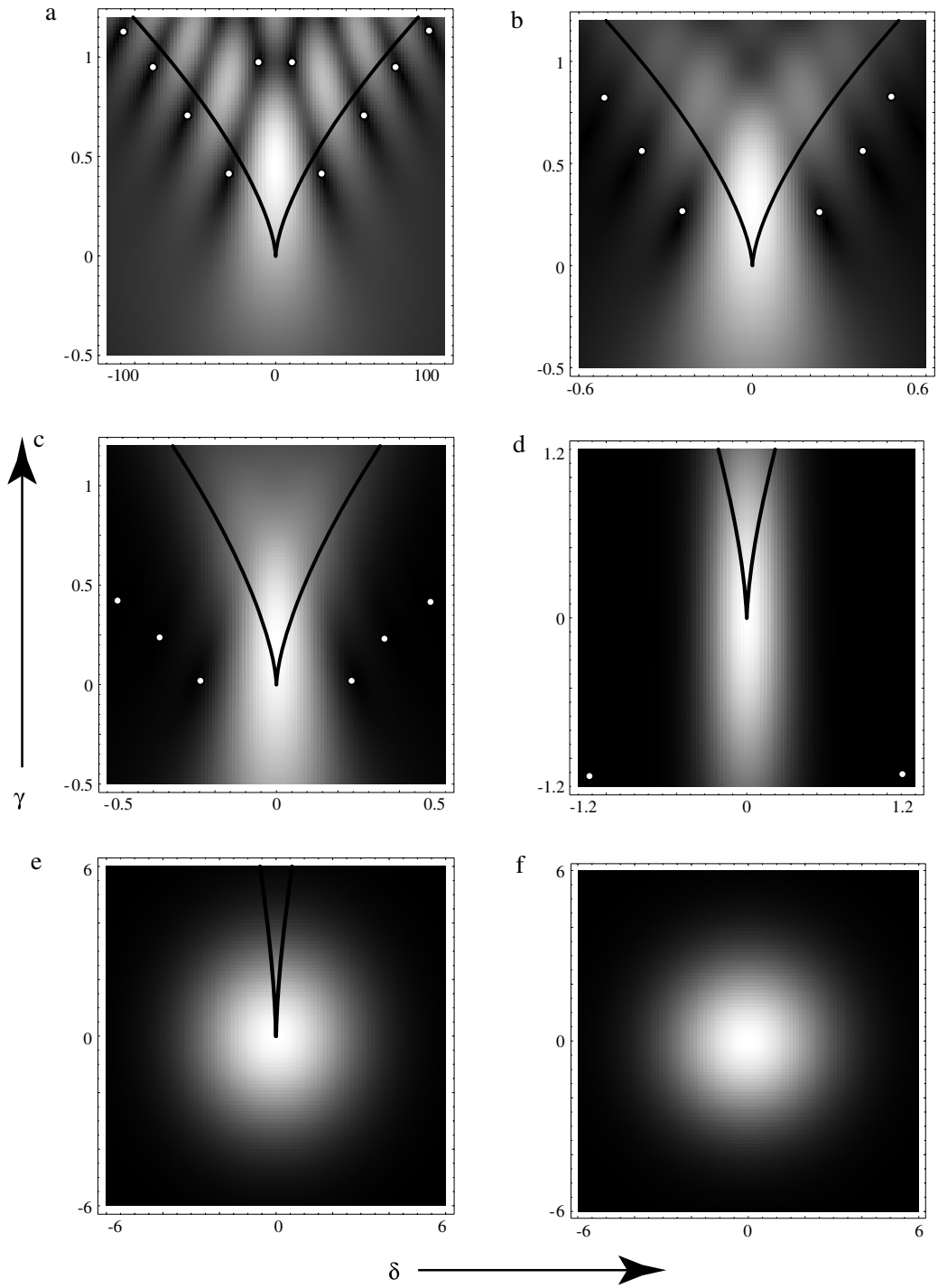

Figure 10. ((a)–(e)) Density plots of far-field cusp intensity $J\ (\gamma, \delta, \sigma, \kappa)$ (equation (35)), with zeros indicated by white dots, for (a) $\sigma = 0.01, \kappa = 10$; (b) $\sigma = 2, \kappa = 10$; (c) $\sigma = 3, \kappa = 10$; (d) $\sigma = 5, \kappa = 5$; (e) $\sigma = 20, \kappa = 0.5$. (f) as for (e), for the large-σ, small-κ approximation (36). The black curves indicate the location of the geometrical caustic.

the saddle-point near $t = 0$. This leads to

$$\left.\begin{aligned} J(\gamma, \delta, \sigma, \kappa) &\approx \kappa^2 \exp\{-(\gamma^2 + \eta^2)\kappa^2\} \\ &= \left(\tfrac{kL}{A}\right)^2 \exp\left\{-(\theta^2 + \phi^2)k^2L^2\right\} \end{aligned}\right\} \quad (\sigma \gg 1, \kappa \ll 1). \tag{36}$$

Figure 10 illustrates how the Pearcey diffraction catastrophe transforms into the Gaussian spot as L decreases, that is as σ increases and κ decreases. As the main diffraction maximum becomes Gaussian, the zeros within the cusp annihilate in pairs and the zeros flanking the cusp recede towards infinity, as noted and explored in detail by Nye [14] for a sharp-edged cylindrical lens; in the two-dimensional case considered here, the details are different: the annihilation is between diagonally, rather than horizontally (constant v) adjacent zeros,

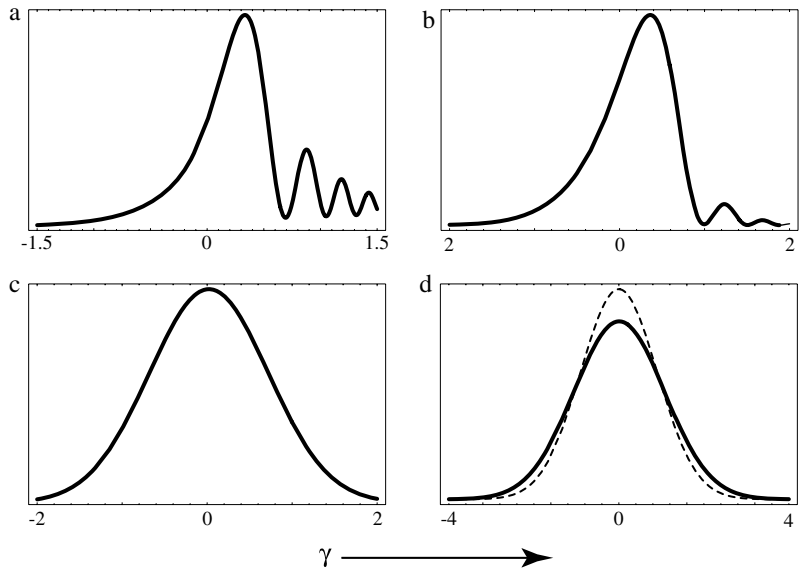

Figure 11. Graphs of $J(\gamma, 0, \sigma, \kappa)$ versus γ. (a) $\sigma = 0.2, \kappa = 20$; (b) $\sigma = 1.5, \kappa = 10$; (c) $\sigma = 7.071, \kappa = 7.071$; (d) $\sigma = 10, \kappa = 0.63$. The dashed curve in (d) is the large-σ, small-κ approximation (36).

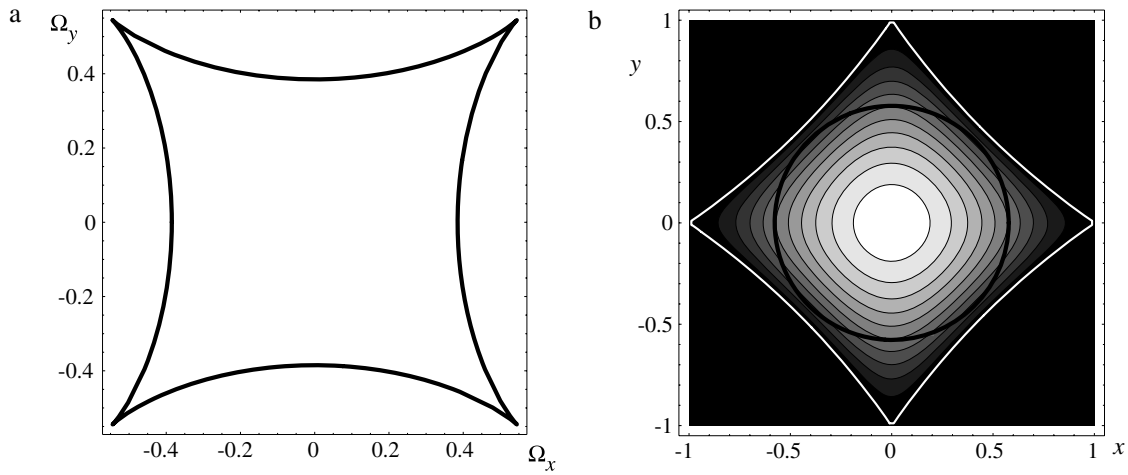

Figure 12. (a) Four-cusped astroid far-field caustic; (b) contour plot of water-drop 'lens' (37), with boundary shown in white; the thick black circle is the locus of zero Gaussian curvature generating the caustic in (a).

and the zeros move directly towards their annihilation, rather than initially spiralling away from their Pearcey locations as in [14]. Figure 11 shows more detail of the 'Gaussianization', as κ decreases and σ increases, in the form of sections through the image for $\delta = 0$ (note that parameters are different from those in figure 10).

7. Numerical illustration for fold and cusp

Consider looking at the four-cusped astroid caustic (figure 12(a)) produced by a water-drop lens with a sharp-cornered boundary with square symmetry (figure 12(b)) [22], held close to the eye; this is a model for looking at a distant light through raindrops on spectacle lenses, or at the far-field caustic generated by shining a Gaussian beam through the drop. The profile of the droplet, satisfying the equation for equilibrium under surface tension, can be written using dimensionless coordinates as (cf equation (18) of [22] for $n = 4$)

$$h(x, y) = \text{constant} - \tfrac{1}{2}(x^2 + y^2) + \tfrac{1}{4}(x^4 - 6x^2y^2 + y^4). \quad (37)$$

The far-field caustic is the image of the circle $x^2 + y^2 = \frac{1}{3}$ of zero Gaussian curvature, with parametric representation

$$\left.\begin{aligned} \Omega_x &= -3^{-1/2}\cos\phi + 3^{-3/2}\cos 3\phi \\ \Omega_y &= -3^{-1/2}\sin\phi - 3^{-3/2}\sin 3\phi \end{aligned}\right\} \qquad (0 \leqslant \phi < 2\pi). \quad (38)$$

One of the four cusps is generated from $x = y = 1/\sqrt{6}$, and an intersection with the fold is generated from $x = 1/\sqrt{3}$, $y = 0$. The four-cornered boundary of the drop is the contour $h(x, y) = -1/4$. (The circle of zero Gaussian curvature lies within this boundary; if instead we had chosen the cubic function $h(x, y)$, generating a three-cusped astroid [23], the circle would touch the boundary, giving rise to an unwanted aperture effect irrelevant to the one considered here.)

Reverting to physical coordinates, and choosing a droplet with maximum thickness H and diameter (distance between opposite corners) D, then local expansion about $x = y = 1/\sqrt{6}$, and rotation of coordinates, generates the model cusp (27), with constants A and B, and hence dimensionless parameters κ and σ from (30). A measure of resolution is, from (33), σ^2/κ; this is small for good resolution and large for poor resolution. These quantities are

$$A = \frac{D^2}{2H}, \qquad B = \sqrt{\frac{D^3}{8H\sqrt{6}}}, \qquad \kappa = \frac{2L^2Hk}{D^2}, \qquad \sigma = \frac{1}{2^{5/4}3^{1/4}}\sqrt{\frac{D}{L}}. \tag{39}$$

For the fold, local expansion about $x = 1/\sqrt{3}$, $y = 0$ generates the model (19), enabling identification of the constant A, and dimensionless parameter κ from (21), as

$$A = \frac{1}{2^{7/4}3^{1/4}}\sqrt{\frac{D^3}{H}}, \qquad \kappa = 8\sqrt{6}\frac{HL^3k}{D^3}. \tag{40}$$

For red light, and a typical drop with clearly-visible caustics, we can take $D = 2$ mm and $H = 0.1$ mm; then, with $L = 2$ mm, we find $\kappa \approx 2000$, $\sigma \approx 0.32$ and $\sigma^2/\sqrt{\kappa} \approx 0.002$ for the cusp, and $\kappa \approx 19\,500$ for the fold. So these caustics are effectively perfectly resolved. For poor resolution, we can reduce the aperture (e.g. Gaussian beam width) to $L = 50\ \mu$m; then $\kappa \approx 1.24$, $\sigma \approx 2$ and $\sigma^2/\sqrt{\kappa} \approx 3.7$ for the cusp, and $\kappa \approx 0.3$ for the fold.

Acknowledgments

I am grateful to the Centre for Theoretical Studies at the Indian Institute of Technology, Kharagpur, for hospitality while the first draft of this paper was written. I thank Professors P Shukla and J F Nye and Dr M Dennis for helpful comments and suggestions.

References

[1] Born M and Wolf E 2005 *Principles of Optics* (London: Pergamon)
[2] Longuet-Higgins M S 1960 Reflection and refraction at a random moving surface. I. Pattern and paths of specular points *J. Opt. Soc. Am.* **50** 838–44
[3] Longuet-Higgins M S 1960 Reflection and refraction at a random moving surface. II. Number of specular points in a Gaussian surface *J. Opt. Soc. Am.* **50** 845–50
[4] Longuet-Higgins M S 1960 Reflection and refraction at a random moving surface. III. Frequency of twinkling in a Gaussian surface *J. Opt. Soc. Am.* **50** 851–6
[5] Petters A O, Levine H and Wambsganss J 2001 *Singularity Theory and Gravitational Lensing* (Boston, MA: Birkhäuser)
[6] Berry M V and Upstill C 1980 Catastrophe optics: morphologies of caustics and their diffraction patterns *Prog. Opt.* **18** 257–346
[7] Nye J F 1999 *Natural Focusing and Fine Structure of Light: Caustics and Wave Dislocations* (Bristol: Institute of Physics Publishing)
[8] Toscano F and Ozorio de Almeida A O 1999 Geometrical approach to the distribution of the zeros of the Husimi function *J. Phys. A: Math. Gen.* **32** 6321–46
[9] Marcuse D 1972 *Light Transmission Optics* (New York: Van Nostrand)
[10] Goodman J W 1985 *Statistical Optics* (New York: Wiley–Interscience)
[11] Berry M V and Wright F J 1980 Projection identities for diffraction catastrophes *J. Phys. A: Math. Gen.* **13** 149–60
[12] Hentschel M, Schomerus H and Schubert R 2003 Husimi functions at dielectric interfaces: inside-outside duality for optical systems and beyond *Europhys. Lett.* **62** 636–42
[13] Nye J F 2003 From Airy rings to the elliptic umbilic diffraction catastrophe *J. Opt. A: Pure Appl. Opt.* **5** 503–10
[14] Nye J F 2003 Evolution from a Fraunhofer to a Pearcey pattern *J. Opt. A: Pure Appl. Opt.* **5** 495–502
[15] Nye J F 2006 Evolution of the hyperbolic umbilic diffraction pattern from Airy rings *J. Opt. A: Pure Appl. Opt.* **8** 304–14
[16] Berry M V 1977 Focusing and twinkling: critical exponents from catastrophes in non-Gaussian random short waves *J. Phys. A: Math. Gen.* **10** 2061–81
[17] Abramowitz M and Stegun I A 1972 *Handbook of Mathematical Functions* (Washington, DC: National Bureau of Standards)
[18] Jaroszynski M and Paczynski B 1995 Diffraction effects in microlensing of Q2237 + 0305 *Astrophys. J.* **455** 443–7
[19] Peterson J B and Falk T 1991 Gravitational lens interference *Astrophys. J.* **374** L5–8
[20] Ulmer A and Goodman J 1995 Femtolensing: beyond the semiclassical approximation *Astrophys. J.* **442** 67–75
[21] Lee R and Fraser A 2001 *The Rainbow Bridge: Rainbows in Art, Myth and Science* (Bellingham, WA: Pennsylvania State University and SPIE Press)
[22] Berry M V 1976 Waves and Thom's theorem *Adv. Phys.* **25** 1–26
[23] Berry M V, Nye J F and Wright F J 1979 The elliptic umbilic diffraction catastrophe *Phil. Trans. R. Soc.* A **291** 453–84
[24] Pearcey T 1946 The structure of an electromagnetic field in the neighbourhood of a cusp of a caustic *Phil. Mag.* **37** 311–7